

Site-specific atomic substitution in a giant magnetocaloric Fe_2P -type system

Sagar Ghorai,¹ Johan Cedervall,² Rebecca Clulow,³ Shuo Huang,^{4,5} Tore Ericsson,³ Lennart Häggström,³ Vitalii Shtender,³ Erna K. Delczeg-Czirjak,⁶ Levente Vitos,⁵ Olle Eriksson,⁶ Martin Sahlberg,³ and Peter Svedlindh¹

¹*Department of Materials Science and Engineering, Uppsala University, Box 35, SE-751 03, Uppsala, Sweden**

²*Department of Materials and Environmental Chemistry, Stockholm University, SE-10691 Stockholm, Sweden*

³*Department of Chemistry – Ångström Laboratory, Uppsala University, Box 538, Uppsala, 75121, Sweden*

⁴*Faculty of Materials Science and Chemistry, China University of Geosciences, Wuhan 430074, China*

⁵*Department of Materials Science and Engineering, Royal Institute of Technology, Stockholm SE-100 44, Sweden*

⁶*Department of Physics and Astronomy, Uppsala University, Box 516, SE-751 20 Uppsala, Sweden*

(Dated: September 30, 2022)

Giant magnetocaloric (GMC) materials constitute a requirement for near room temperature magnetic refrigeration. $(Fe,Mn)_2(P,Si)$ is a GMC compound with strong magnetoelastic coupling. The main hindrance towards application of this material is a comparably large temperature hysteresis, which can be reduced by metal site substitution with a nonmagnetic element. However, the $(Fe,Mn)_2(P,Si)$ compound has two equally populated metal sites, the tetrahedrally coordinated $3f$ and the pyramidally coordinated $3g$ sites. The magnetic and magnetocaloric properties of such compounds are highly sensitive to the site specific occupancy of the magnetic atoms. Here we have attempted to study separately the effect of $3f$ and $3g$ site substitution with equal amounts of vanadium. Using formation energy calculations, the site preference of vanadium and its influence on the magnetic phase formation are described. A large difference in the isothermal entropy change (as high as 44%) with substitution in the $3f$ and $3g$ sites is observed. The role of the lattice parameter change with temperature and the strength of the magnetoelastic coupling on the magnetic properties are highlighted.

I. INTRODUCTION

Replacement of conventional vapour compression refrigeration with a 20–30% more efficient solid state magnetic refrigeration technique based on the magnetocaloric effect has the additional advantage of reducing emission of greenhouse gases [1]. To build a magnetic refrigerator which can work near room temperature, materials with a giant magnetocaloric (GMC) effect and a magnetic phase transition temperature near room temperature are required. In this regard, several GMC materials with first order magnetic phase transitions have been proposed [2]. Despite of high values of the isothermal entropy change and adiabatic temperature change, these first order materials may not be suitable for magnetic refrigeration owing to a large temperature hysteresis (ΔT_{hys}). ΔT_{hys} represents the irreversible nature of the temperature dependent magnetic phase change, which is a drawback for magnetic refrigeration [3]. While several ways of reducing ΔT_{hys} have been attempted [3, 4], the basic origin of ΔT_{hys} is still unclear. Here in this work we provide an explanation for the origin of ΔT_{hys} in the context of magnetoelastic coupling of $(Fe,Mn)_2(P,Si)$ -type materials. $(Fe,Mn)_2(P,Si)$ -type materials constitute a class of GMC materials consisting of earth abundant, environment friendly and non-toxic elements. These compounds crystallize in a hexagonal Fe_2P -type structure (space group $P\bar{6}2m$). In the hexagonal structure the metallic atoms occupy the $3f$ and $3g$ sites while the non metallic atoms occupy the $1b$ and $2c$ sites [5, 6]. From

electronic structure calculations [7], the observed magnetoelastic coupling for this series of compounds has been explained by a drastic fall of the magnetic moment of Fe ($1.54\mu_B$ /atom to $\sim 0.003\mu_B$ /atom) while it transforms from the ferromagnetic (FM) to the paramagnetic (PM) state. This moment change occurs due to the fact that the non-bonded or metallic Fe below the Curie temperature (T_C) hybridizes with Si/P above T_C . The hybridization around T_C causes a drastic change of the hexagonal lattice parameters and a strong magnetoelastic coupling results [7]. For GMC materials, a high magnetization is beneficial, which is mainly provided by the Mn atoms. It can be stated as that the Fe atoms maintain the first order phase transition, while Mn atoms maintain the overall magnetization of $(Fe,Mn)_2(P,Si)$ -type materials. To understand the effect of these two phenomena, Fe and Mn atoms are individually attempted to be replaced with non-magnetic V in this work. Recently Lai et al. [8, 9] have discussed the reduction of ΔT_{hys} with V substitution in the metallic sites. However, the occupation of V in the metallic sites (i.e. $3f$ or $3g$ sites) is still unclear. Interestingly, the magnetic atoms exhibit different magnetic moments depending upon their site occupancy [10], yielding completely different magnetic and magnetocaloric properties (e.g. T_C , saturation magnetization (M_S), isothermal entropy change ($-\Delta S_M$), ΔT_{hys} etc.). Here, in this work we have attempted to substitute the $3g$ and $3f$ sites of the parent compound $FeMnP_{0.5}Si_{0.5}$ individually with 5 at% of V. Both site substitutions exhibit small difference in the T_C values, while there is a large difference ($\sim 44\%$ at $\mu_0 H = 2T$) in the value of $-\Delta S_M$. This difference is explained by the strength of the magnetoelastic coupling and the preferred occupancy

* sagar.ghorai@angstrom.uu.se

of V.

II. EXPERIMENTAL DETAILS AND CALCULATION METHOD

All compounds were synthesized by the drop synthesis method [11]. Further, the vacuum sealed samples (pressed pellets) were sintered at 1373 K for 1 hr, followed by annealing at 1073 K for 65 hrs before quenched in ice water. X-ray powder diffraction (XRPD) data were collected at different temperatures ranging from 265 K to 422 K using a Bruker D8 Advance diffractometer with Cu-K $_{\alpha 1}$ radiation, with an angle step size of 0.02°. Variable temperature XRD data were analysed using Pawley refinements within the topas 6 software program [12]. Mössbauer measurements were carried out on a constant acceleration spectrometer with a $^{57}\text{CoRh}$ source. The samples were enclosed in sealed kapton pockets yielding a sample concentration of ≈ 10 mg/cm 2 . Calibration spectra were recorded at 295 K using natural Fe metal foil as a reference absorber. The spectra were recorded at 410 K and fitted using the least square Mössbauer fitting program Recoil to obtain the values of the center shift CS , the magnitude of the electric quadrupole splitting $|QS|$, the full-width at half maxima W of the Lorentzian absorption lines and the spectral intensities I . Magnetic properties were measured in the temperature range from 5K to 400K using Quantum Design MPMS-XL and PPMS systems with a maximum magnetic field of 5T. EDX (energy dispersive X-ray) measurements were performed on a Zeiss Leo 1550 field emission SEM (scanning electron microscope) equipped with Aztec energy dispersive X-ray detector. Data were collected on at least 10 spots of each sample using an accelerating voltage of 20 kV by and EDx mapping was carried out on regions of approximately 300 $\mu\text{m} \times 300 \mu\text{m}$.

The total energy calculations were carried out by the exact muffin-tin orbitals (EMTO) method in combination with the coherent potential approximation (CPA) [13]. The one-electron Kohn-Sham equation was solved within the soft-core and scalar-relativistic approximations. The s , p , d and f orbitals were included in the muffin-tin basis set. The Green's function was calculated by using 16 complex energy points on a semicircular contour including the valence states. The exchange-correlation interactions were treated within the generalized gradient approximation in the form of Perdew-Burke-Ernzerhof (PBE) [14]. Further details about the adopted method can be found in previous work [13]. For the further discussion the parent compound, $\text{FeMnP}_{0.5}\text{Si}_{0.5}$ and the two V substituted compounds $\text{FeMn}_{0.95}\text{V}_{0.05}\text{P}_{0.5}\text{Si}_{0.5}$ (3g site substituted) and $\text{Fe}_{0.95}\text{V}_{0.05}\text{MnP}_{0.5}\text{Si}_{0.5}$ (3f site substituted) are abbreviated as P, V3g, and V3f, respectively.

III. RESULTS AND DISCUSSION

A. Magnetoelastic coupling and magnetocaloric effect

The magnetocaloric effect is often characterized with the isothermal entropy change ($-\Delta S_M$). The total entropy of a system is the sum of magnetic, lattice and electronic entropy contributions of the system. For a first order magnetic phase transition (i.e. a system with a discontinuity in the first order derivative of the Gibbs free energy) the magnetic phase transition is often associated with a lattice or electronic phase transition. Moreover, if this is the case, a high value of $-\Delta S_M$ is expected.

The $(\text{Fe,Mn})_2(\text{P,Si})$ -system shows a first order magnetoelastic phase transition, where a sharp change of the hexagonal lattice parameter ratio c/a (keeping the lattice volume almost constant) occurs in the vicinity of the magnetic phase transition. Hence, the total entropy change of the system includes by both magnetic and lattice entropy contributions. In our studied compounds a temperature dependent change of the c/a ratio from a high value (~ 0.57) to a relatively lower value (~ 0.53) has been observed when the system transforms from the PM to the FM state. At high temperature ($> T_C + 30$ K) the system corresponds fully to a Fe_2P -type phase with a high c/a ratio, while at a sufficiently low temperature ($< T_C - 100$ K) the system corresponds fully to a Fe_2P -type phase with a low c/a ratio. Therefore, near T_C , contributions (phase wt%) from both Fe_2P -type phases with high and low c/a ratios are present. From the collected XRPD patterns, the temperature dependent variation of two Fe_2P -type phases are shown in Fig.1(a). The crossing point of the two Fe_2P phases represent the c/a transition temperature, i.e. the structural phase transition temperature (T_{st} , cf. Fig.1(a)). The strength of the magnetoelastic coupling depends upon two factors; firstly the degree of structural change, in this case the variation of the c/a ratio, which is shown in the inset of Fig.1(a), and secondly the difference between the structural and magnetic phase transition temperatures. From the relative difference between T_{st} and T_C (cf. Fig.1(a)) and the change of absolute value of c/a (cf. inset of Fig.1(a)), it is clear that the magnetoelastic coupling strength is highest for parent compound (P) followed in descending order by the V3g and V3f compounds. As discussed before, the strength of magnetoelastic coupling has a direct influence on the value of $-\Delta S_M$. The value of $-\Delta S_M$ has been calculated using the Maxwell relation [15], $\Delta S_M(T, H_f) = \mu_0 \int_0^{H_f} (\frac{\delta M(H, T)}{\delta T})_H dH$, for a magnetic field change of H_f . The magnetic isotherms have been recorded during cooling of the material with a cyclic measurement protocol [16], where the sample is subsequently heated to its PM state before stabilizing at the temperature of the measurement. The calculated values of $-\Delta S_M$ are presented in Fig.1(b). The values of $-\Delta S_M$ follows the same trend as that of the magnetoelastic coupling strength, i.e. the highest value for parent

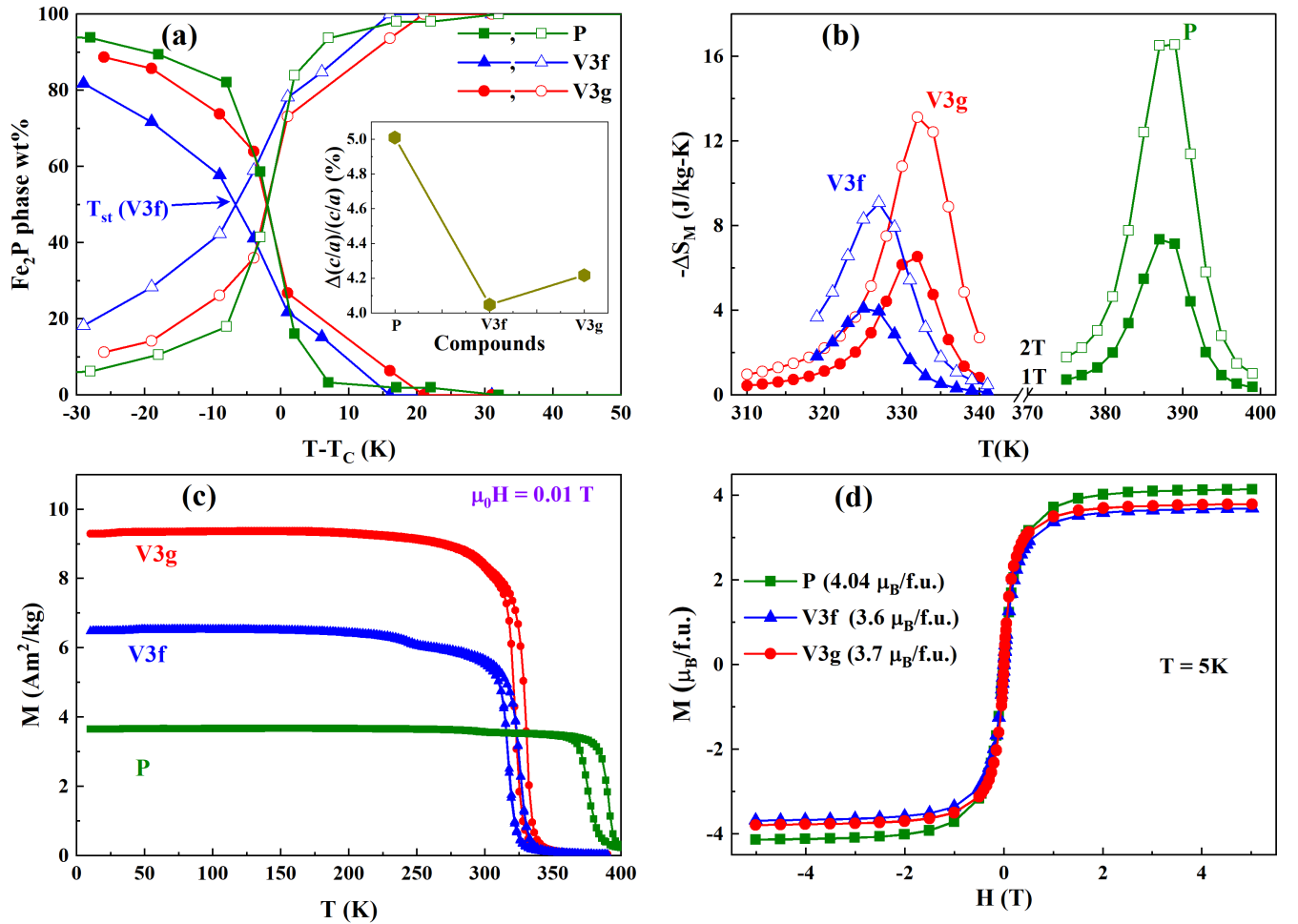


FIG. 1. (a) Temperature dependent variation of Fe₂P phases with low (~ 0.53) and high (~ 0.57) c/a ratios represented by solid and hollow symbols, respectively. The crossing points of the two Fe₂P phases represent structural transition temperature T_{st} (for V3f compound, the blue arrow indicates the T_{st}) of the studied compounds. The inset shows the relative variation of c/a for the different compounds transforming from the PM to the FM state. (b) Temperature dependent variation of the isothermal entropy change, hollow (solid) symbols represent data at a magnetic field change of 2 T (1 T). (c) Temperature dependent variation of magnetization at $\mu_0 H = 0.01$ T. (d) Isothermal magnetization at 5 K.

compound followed by lower values of the V3g and V3f compounds. This is a manifestation of the proportionality between the magnetoelastic coupling strength and $-\Delta S_M$.

To estimate the temperature range of the materials to be useful as a magnetic refrigerant, the relative cooling power (RCP) is often used [17]. The RCP value can be calculated from the temperature dependent $-\Delta S_M$ curve as $RCP = -\Delta S_M^{max} \times \Delta T_{FWHM}$, where $-\Delta S_M^{max}$ is the maximum of the isothermal entropy change and ΔT_{FWHM} is the full width at half maximum of the temperature dependent $-\Delta S_M$ curve. Here the RCP and $-\Delta S_M$ values of the studied compounds along with the corresponding data for some well known GMC materials are listed in Table I.

B. Curie temperature and hysteresis

For a material to be useful in room-temperature magnetic refrigeration, the first requirement is to have a magnetic phase transition temperature near room temperature. The parent compound (FeMnP_{0.5}Si_{0.5}) has a T_C value of around 380 K. With 5 at% V substitution in either of the metallic sites (we will discuss later that V prefers the 3g site), T_C decreases and comes closer (~ 320 K) to room temperature (cf. Fig1(c)), making this substitution process useful for magnetic refrigeration. The value of T_C corresponds to the amount of thermal energy required to transform a material from its magnetically ordered state to a magnetically disordered state, therefore the value of T_C is directly related with the strength of the exchange interaction between the spins of the magnetic atoms. Moreover, the exchange interaction between spins

TABLE I. Magnetocaloric properties of the studied compounds (*) compared with data reported for other GMC materials near room temperature.

Sample	T_C^{FC} (K)	$\mu_0 H$ (T)	$-\Delta S_M$ (J/kgK)	RCP (J/kg)	Ref.
FeMnP _{0.5} Si _{0.5} (P)	376	2	16.5	147	*
Fe _{0.95} V _{0.05} MnP _{0.5} Si _{0.5} (V3f)	318	2	9.1	103	*
FeMn _{0.95} V _{0.05} P _{0.5} Si _{0.5} (V3g)	322	2	13.1	130	*
Gd	295	2	6.1	240	[18]
La(Fe _{0.98} Mn _{0.02}) _{11.7} Si _{1.3} H	312	2	13	-	[19]
La _{0.67} Ca _{0.33} MnO ₃	260	1.5	4.3	47	[20]
La _{0.5} Pr _{0.2} Ca _{0.1} Sr _{0.2} MnO ₃	296	2	1.8	147	[21]
Fe ₈₀ Pt ₂₀	290	2	~ 10	-	[22]
Mn _{1.2} Fe _{0.8} P _{0.75} Ge _{0.25}	288	2	20	-	[23]
MnFeP _{0.52} Si _{0.48}	268	2	10	-	[24]

is highly sensitive to the inter spin distance. From neutron diffraction [5, 6] and Mössbauer spectroscopy [25] results, it has been observed that in the (Fe,Mn)₂(P,Si) system, Fe, Mn and P / Si occupy the $3f$, $3g$ and $1b$ / $2c$ sites of the hexagonal lattice, respectively. Among them, the magnetic atoms Fe and Mn are separated along the c -axis and distributed in the ab -plane. Hence, the distance along the c -axis represents the distance between Fe and Mn atoms. From temperature dependent XRPD results, the variation of the lattice parameter c with temperature for every compound is depicted in Fig 2(a). It should be kept in mind that near T_C all compounds have two Fe₂P-type phases with different c/a ratio. Among them the low c/a ratio is dominant below T_C and vice versa. Therefore, in the following discussion only the dominant Fe₂P-phase is considered. From Fig.2(a), it is observed that when the material transforms from PM to FM state, there is a large decrease (for the dominant Fe₂P phase) of the lattice parameter c , indicating a decrease of the Fe to Mn atomic distance. From TableII and inset of Fig.2(a), it is clear that the largest relative change of the c -parameter ($\Delta c/c$) has been observed for the parent compound, followed by the compounds V3g and V3f in descending order. As expected, the T_C values show the same trend. It can be concluded that the smaller the Fe to Mn distance along the c -axis, the stronger the exchange coupling strength is and hence T_C is inversely proportional to the Fe to Mn distance.

TABLE II. Magnetic and magnetoelastic properties.

Sample	T_C^{FC} (K)	$\Delta c/c$ (%)	$\Delta a/a$ (%)	ΔT_{hys} (K)	M_S ($\mu_B/f.u.$)
P	376	3.30	1.64	22	4.04
V3f	318	2.64	1.34	8.5	3.6
V3g	322	2.80	1.44	8.5	3.7

Apart from the variation of lattice parameter c , the temperature dependent variation of the a lattice param-

eter is shown in Fig.2 (b). For the PM to FM phase transition a sharp increase of the a -parameter is observed. Now, Fe and Si both occupy the same basal plane, thus an increase of the a -parameter favors localization of the $3d$ electrons and less bonding with Si atoms. From DFT calculation results [7, 26] of (Fe,Mn)₂(P,Si)-system, it has been observed that the density of states (DOS) of Mn $3d$ electrons remains identical in the FM and PM states while the DOS of the Fe $3d$ electrons is significantly different comparing the FM and PM states. In fact the change of the local magnetic moment of Fe has been identified as the reason for observing the magnetoelastic coupling in the (Fe,Mn)₂(P,Si)-system [27]. Moreover, the increment of the a lattice parameter, across the PM to FM transition represents a strong magnetoelastic coupling. Similar to the variation of the c -parameter, the variation of a ($\Delta a/a$, see TableII) is also largest for the parent compound, followed by the V3g and V3f compounds. The large change of the lattice parameters a and c close to the magnetic transition is the reason for observing a strong first order magnetic phase transition for these materials. The two Fe₂P-type phases, characterized by different a and c parameters are separated by an energy barrier, which is responsible for the temperature hysteresis (ΔT_{hys}) of these materials [28]. TableII shows the variation of the lattice parameters ($\Delta a/a$ and $\Delta c/c$) across the magnetic transition indicating that the parent compound has the strongest magnetoelastic coupling or largest energy barrier, resulting in a relatively larger value of ΔT_{hys} . On the contrary, the relatively lower values of $\Delta a/a$ and $\Delta c/c$ for the V3f and V3g compounds yield reduced values of ΔT_{hys} . For the reversibility of a magnetic heat pump, a minimal value of ΔT_{hys} is required[3], indicating that V substitution constitutes a useful process for magnetic refrigeration applications.

C. Magnetization anomaly and Mössbauer spectra

Theoretical calculations of the site specific magnetic moment of the parent compound (FeMnP_{0.5}Si_{0.5}) show that the magnetic moments of Mn in the $3g$ site and Fe in the $3f$ site are $2.81 \mu_B/\text{atom}$ and $1.68 \mu_B/\text{atom}$, respectively [10]. Therefore, substitution with nonmagnetic V is expected to reduce the overall magnetization more for $3g$ -site substitution compared to $3f$ -site substitution. However, an inverse behaviour is observed from the values of the saturation magnetization (cf. Fig1(d) and TableII). A possible reason of this anomaly could be a partly random occupancy of Fe and Mn atoms, i.e. if some amount of Fe (Mn) is distributed in the $3g$ ($3f$) site. To investigate this possibility, we have collected Mössbauer spectra for the compounds in their paramagnetic states.

In Fig.3, the Mössbauer spectra of the three studied compounds are shown. For the parent compound, FeMnP_{0.5}Si_{0.5}, the broadenings emanate from the different surroundings of Fe at the metal $3f$ site. There

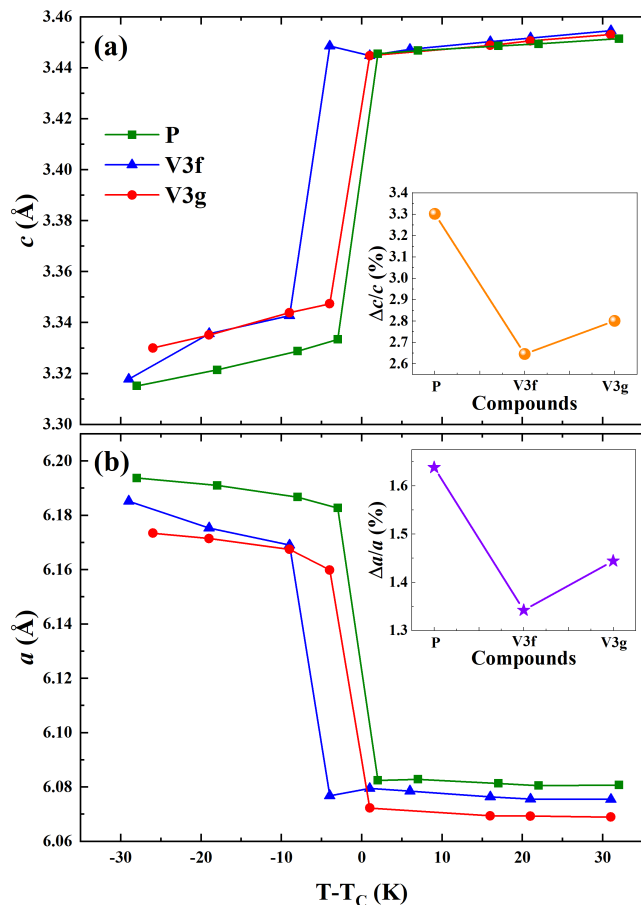


FIG. 2. Temperature dependent variation of the hexagonal lattice parameters; (a) c and (b) a considering only the dominant Fe_2P -phase. The inset shows the relative variation of the lattice parameters at T_C . See supplementary for details. The error in the lattice parameter data is in the order of 10^{-4} Å, therefore not included in the figure.

are four near neighbours elements P and Si, two occupying the $1b$ and two the $2c$ sites. It has been shown that Si prefers the $2c$ site almost exclusively [29]. For the present compound, two P atoms will occupy the two nearest $1b$ sites and assuming random occupation on the $2c$ sites we would expect three different near neighbour surroundings; P_2Si_2 (i.e. one Fe atom is surrounded by two P and two Si atoms), P_3Si_1 and P_4 with probabilities of 0.5625, 0.375, and 0.0625, respectively. These components are shown in Fig.3 with red, green and blue sub-patterns, respectively. Accordingly, the spectra at 410 K, irrespective of V content were fitted with three doublets. The fitting results for the average hyperfine values are presented in Table III. The CS values for the V substituted samples have decreased as compared to the value for the parent sample. It should be noted that a decrease in CS corresponds to an increase in electron density at the Fe nuclei. This decrease in CS can therefore be associated with the shrinking of the a -axis for the

TABLE III. Results from fitting of Mössbauer spectra.

Sample	CS (± 0.005)	$ QS $ (± 0.005)	W (± 0.005)
P	0.220	0.210	0.406
V3g	0.193	0.336	0.558
V3f	0.185	0.279	0.443

V substituted samples making the P and Si atoms in the first coordination sphere coming closer to the Fe nuclei. As discussed before, a higher value of the a -parameter prevents Fe bonding with non-metallic atoms and yields the desired moment fluctuation across the PM to FM phase transition. A larger moment fluctuation will result in a larger change of magnetic entropy and hence a larger value of $-\Delta S_M$. The same trend for the values of CS and $-\Delta S_M$ confirms the theoretical prediction [27] of the moment fluctuation of Fe in the $3f$ site.

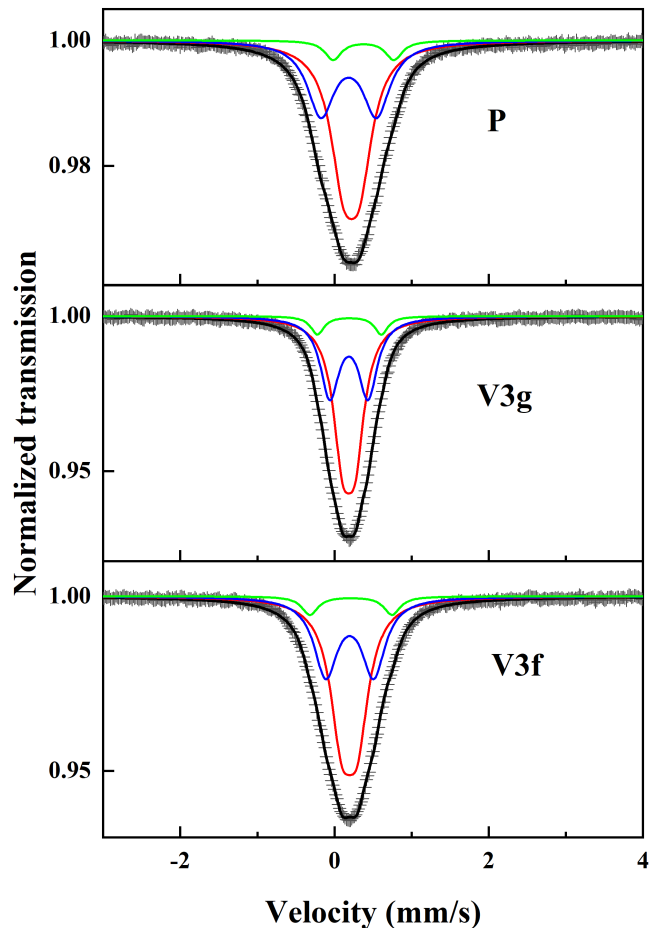


FIG. 3. Mössbauer spectra of the studied compounds at 410K. The red, blue and green sub-patterns correspond to the nearest neighbour surroundings (P_2Si_2), (P_3Si_1) and (P_4) of Fe at the $3f$ site, respectively.

The broad single line centered around 0.2 mm/s matches well with results from a previous study [10] and

evidences that Fe atoms occupy the $3f$ site. Also, the absence of any high velocity resonance line or shoulder diminishes the possibility of Fe $3g$ site occupation.

D. Chemical composition and magnetic phases

The chemical compositions of the compounds as obtained from analysis of the EDX results are listed in TableIV.

TABLE IV. Chemical composition of the studied compounds from EDX analysis.

Element (at%)	P	V3 <i>f</i>	V3 <i>g</i>
Fe (expected)	33.33	31.67	33.33
Fe (observed)	33(3)	31(2)	31(2)
Mn (expected)	33.33	33.33	31.67
Mn (observed)	35(3)	34(2)	31(1)
V (expected)	0	1.67	1.67
V (observed)	0	1.9(6)	1.7(2)
P (expected)	16.67	16.67	16.67
P (observed)	16(3)	16(3)	18(2)
Si (expected)	16.67	16.67	16.67
Si (observed)	15(2)	17(2)	19(2)

From TableIV it is clear that all the compounds have the expected chemical composition within the margin of error. However, during analysis of the EDX results some Si-rich portions have been identified. As indicated in the supplementary section, from the elemental mapping of P it is clear that the above mentioned Si-rich portions exhibit P-deficiency. Typically, these Si-rich or P-deficient portions (cf. Fig.4 (a)-(c)) correspond to a (Fe,Mn)₃Si phase. From the room temperature XRPD analysis a small amount (~ 5 at%) of (Fe,Mn)₃Si phase has been identified for the three compounds. Formation of this secondary phase indicates a possible loss of P during synthesis. However, the analysis of the EDX results exhibits a large error bar (as high as 3 at% for the Fe and Mn content) and the XRPD refinement with multiple phases is not very sensitive to Fe/Mn intermixing. Fortunately, the magnetic properties of the secondary phase can be used to predict the Fe to Mn ratio. The (Fe,Mn)₃Si-type phase exhibits a transition to a ferromagnetic state at high temperature along with a low temperature (< 50 K) anti-ferromagnetic type spin-reorientation temperature (T_R). Without Mn, the Fe₃Si phase has a T_C value of around 800 K and with Mn insertion T_C rapidly decreases to values below room temperature [30, 31]. A magnetic phase diagram using literature values of the (Fe,Mn)₃Si phase is shown in Fig.4(d) and results of magnetic transition temperatures for the primary and secondary phases of our studied compounds as obtained from temperature dependent magnetization measurements are shown in Fig.4 (e). Comparing the measured transition temperatures of the (Fe,Mn)₃Si phase with the transition temperatures shown in the phase diagram, it can be concluded that

the secondary phase of the V3*f* compound has a higher Mn to Fe ratio compared to the parent and V3*g* compounds. This also indicates that the V3*f* compound has a deficiency of Mn in the primary Fe₂P-type phase. Interestingly, all three compounds have been synthesized using identical conditions. Therefore the loss of Mn in the V3*f* compound should have some intrinsic origin.

E. Phase formation energy

To find the reason of Mn loss in the V3*f* compound and to estimate the effect of V substitution, the total energies of the systems have been calculated using density functional theory. For a more stable compound, the formation energy is expected to be negative and smaller relative to the pure components in their ground state structures. For the calculation two cases have been considered.

Case 1 : All Fe (Mn) atoms occupy $3f$ ($3g$) sites. Therefore, the formation energy for $3f$ site substitution with x amount of V can be represented as,

$$\Delta F_{Fe_{1-x}V_xMnP_{0.5}Si_{0.5}} = E_{Fe_{1-x}V_xMnP_{0.5}Si_{0.5}} - (1-x)E_{Fe} - xE_V - E_{Mn} - 0.5E_P - 0.5E_{Si}.$$

Similarly, the formation energy for $3g$ site substitution will be,

$$\Delta F_{FeMn_{1-x}V_xP_{0.5}Si_{0.5}} = E_{FeMn_{1-x}V_xP_{0.5}Si_{0.5}} - E_{Fe} - (1-x)E_{Mn} - xE_V - 0.5E_P - 0.5E_{Si}.$$

The energy difference between $3f$ and $3g$ site substitution can therefore be expressed as,

$$\Delta F_1 = E_{Fe_{1-x}V_xMnP_{0.5}Si_{0.5}} - E_{FeMn_{1-x}V_xP_{0.5}Si_{0.5}} + xE_{Fe} - xE_{Mn}.$$

The value of ΔF_1 for two different c/a ratios are listed in TableV. Positive values indicate smaller formation energy for $3g$ site substitution. One may also note that the formation energy difference is higher for a higher level of V substitution. All these facts show that V prefers to occupy the $3g$ site.

Case 2 : Although it is known from analysis of the Mössbauer results that Fe prefers the occupy the $3f$ site, we have no direct evidence that Mn can not occupy the $3f$ site. In this particular case a random occupancy of Fe and Mn in the $3f$ and $3g$ sites with V substitution is considered. Moreover, equimolar amounts in the $3f$ and $3g$ sites are considered, i.e. for each 1 mol in total of P and Si, the total amount of Fe, Mn and V in the metallic sites will be 2 mol. Therefore, similar to case 1, the formation energies for $3f$ and $3g$ site substitutions have been calculated and their difference can be expressed as,

$$\Delta F_2 = E_{(Fe_{1-x}V_x)(Fe_{x/2}Mn_{1-x/2})P_{0.5}Si_{0.5}} - E_{(Fe_{1-x/2}Mn_{x/2})(Mn_{1-x}V_x)P_{0.5}Si_{0.5}}.$$

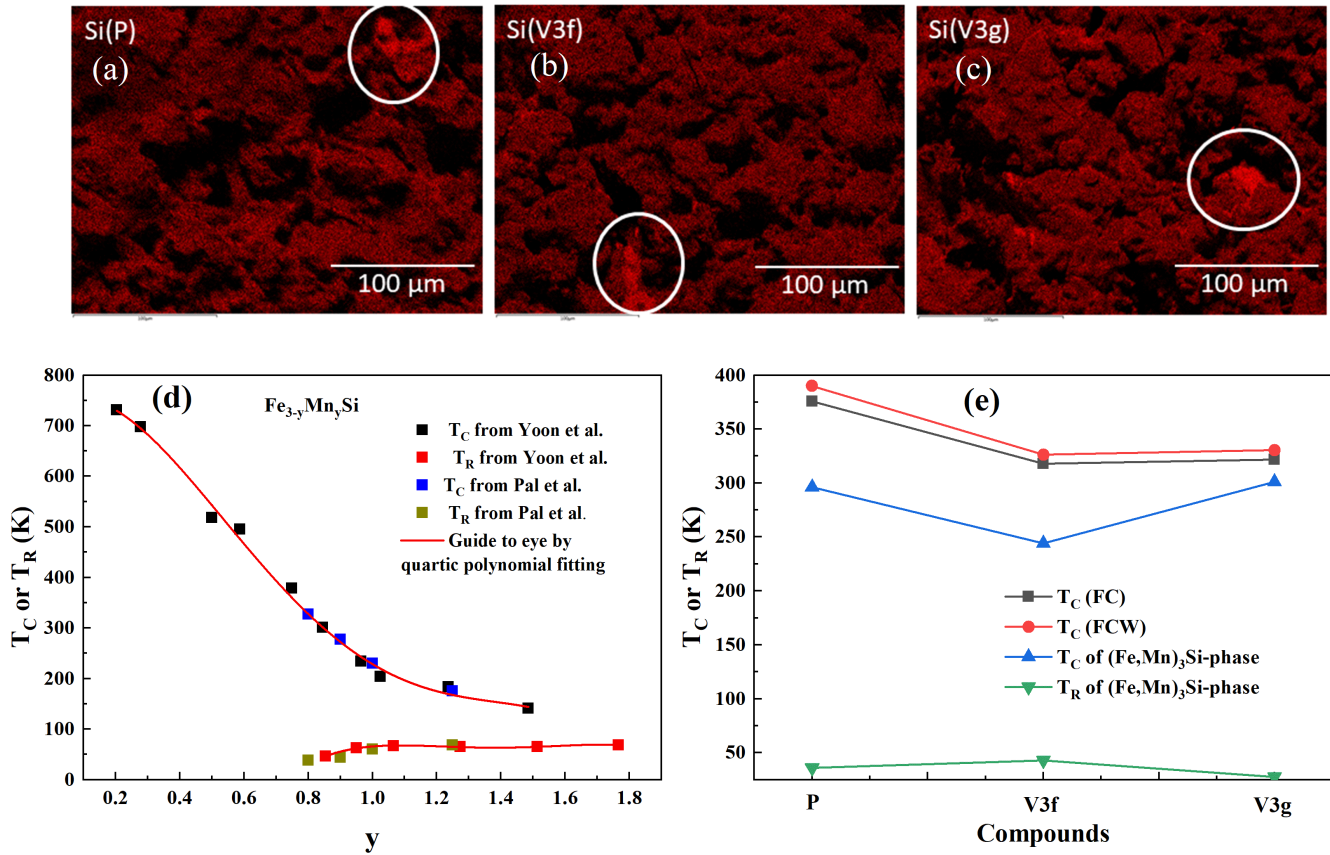


FIG. 4. (a) - (c) Elemental mapping of Si for the three studied compounds. The circled regions indicate regions with excess of Si. (d) Magnetic phase diagram of $Fe_{3-y}Mn_ySi$ based on published literature values for the magnetic ordering temperatures. (e) T_C and T_R values for the primary and secondary phases of the studied compounds.

TABLE V. Results from formation energy calculations. The energy differences are given in units of mRy/atom

x	ΔF_1	ΔF_1	ΔF_2	ΔF_2
	($c/a = 0.53$)	($c/a = 0.58$)	($c/a = 0.53$)	($c/a = 0.58$)
0	0.000	0.000	0.000	0.000
0.01	0.947	0.681	0.949	0.969
0.02	1.797	1.328	1.849	1.391
0.03	2.630	1.946	2.735	2.079
0.04	3.367	2.546	3.511	2.759
0.05	4.182	3.126	4.347	3.373

TableV lists the values of ΔF_2 for two different c/a ratios. Similar to case 1, case 2 also indicates that V prefers to occupy the $3g$ site instead of the $3f$ site. To understand the physical consequences of this, a simplified model (cf. Fig.5) is considered. 10 atoms each of Fe and Mn are considered to occupy the $3f$ and $3g$ sites, respectively as a ground state (i.e. parent compound). Now, if 1 Mn atom is replaced by 1 V atom (i.e. V3g compound), following the total energy minimum criterion, V will occupy the $3g$ state. As a result there will

be equimolar amount of Fe and Mn+V in the $3f$ and $3g$ sites, respectively. However, for the V3f compound, the V atom will not occupy the $3f$ site, it will occupy the $3g$ site. This can have two consequences, either one Mn atom can occupy the $3f$ site or an equimolar amount of metallic atoms will occupy the $3f$ and $3g$ sites and the extra Mn atom will leave the Fe_2P phase and contribute to the secondary phase formation, as indicated in Fig.5. In the first scenario, the Mn in the $3f$ site will interact antiferromagnetically with the Fe in $3f$ site [32]. In the second scenario, some amount of Mn will leave the Fe_2P phase of the V3f compound, and participate in the secondary phase formation, which will enhance the Mn/Fe ratio of the secondary phase ($Fe_{1-x}Mn_xSi$). The enhancement of the Mn/Fe ratio in the V3f compound has been discussed previously. Moreover, in both cases, the overall magnetization of the V3f compound will decrease, which explains the observed magnetization anomaly in the saturation magnetization result.

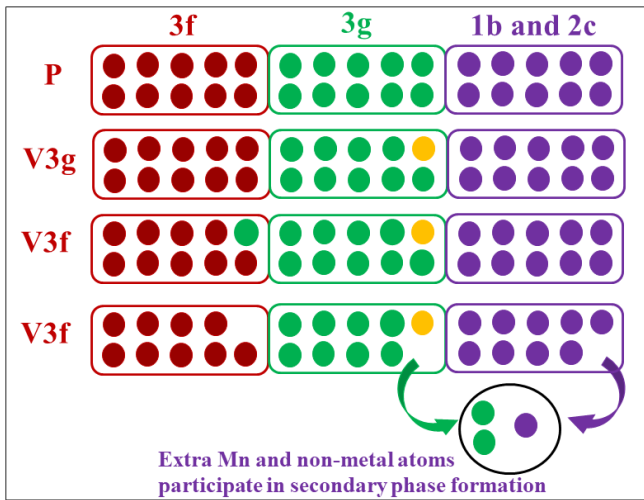


FIG. 5. Model of V (yellow circles) substitution in the Fe (red circles) and Mn (green circles) dominated $3f$ and $3g$ sites, respectively. The purple circles represent P and Si. For the V3f compound two cases with Mn occupying the $3f$ site and Mn leaving the Fe_2P -phase are shown.

IV. SUMMARY AND CONCLUSIONS

V substitution in the metallic sites of $\text{FeMnP}_{0.5}\text{Si}_{0.5}$, results in a decrease of T_C , which is proportional to the magnetic exchange coupling strength. The above mentioned coupling strength is inversely proportional to the Fe to Mn distance along the hexagonal c axis and proportional to the Fe to non-metal (P/Si) distance along the hexagonal a axis. From the formation energy calculations, it was found that $3g$ site substitution is energetically favourable for the V atom. Attempting

a $3f$ site substitution will provoke either antiferromagnetic interaction in the $3f$ -site or a secondary phase formation with the cost of an overall decrease of the magnetization. From Mössbauer spectroscopy of the studied compounds apart from the absence of Fe in the $3g$ site, a decrease of the hyperfine parameter CS (central shift) with V substitution has been observed. A larger CS parameter represents non-bonded or weakly bonded Fe, which is favourable for the Fe moment fluctuation across the PM-FM phase transition [27]. A larger moment fluctuation results in a larger value of $-\Delta S_M$. Therefore, a direct correlation between the CS parameter and the value of $-\Delta S_M$ has been evidenced. Interestingly, the value of the temperature hysteresis ΔT_{hys} decreases with V substitution. The ΔT_{hys} in the Fe_2P -type systems originates from the energy barrier between the states characterized by different c and a lattice parameters (described by $\Delta a/a$ and $\Delta c/c$). Here, in this work we have shown that with V substitution the energy barrier decreases considerably and results in a decrease of ΔT_{hys} , which is highly desirable for the magnetic refrigeration application.

ACKNOWLEDGMENTS

The authors thank the Swedish Foundation for Strategic Research (SSF), project "Magnetic materials for green energy technology" (contract EM-16-0039) for financial support. Financial support from the Swedish Research Council (VR, contract 2019-00645) is gratefully acknowledged. The authors acknowledge support from STandUPP and eSENCE. The computational studies were performed on resources provided by the Swedish National Infrastructure for Computing (SNIC).

-
- [1] K. Gschneidner Jr and V. Pecharsky, International journal of refrigeration **31**, 945 (2008).
 - [2] J. Lyubina, Journal of Physics D: Applied Physics **50**, 053002 (2017).
 - [3] O. Gutfleisch, T. Gottschall, M. Fries, D. Benke, I. Radulov, K. P. Skokov, H. Wende, M. Gruner, M. Acet, P. Entel *et al.*, Philosophical Transactions of the Royal Society A: Mathematical, Physical and Engineering Sciences **374**, 20150308 (2016).
 - [4] L. F. Cohen, physica status solidi (b) **255**, 1700317 (2018).
 - [5] X. Miao, L. Caron, P. Roy, N. Dung, L. Zhang, W. Kockelmann, R. De Groot, N. Van Dijk, and E. Brück, Physical Review B **89**, 174429 (2014).
 - [6] X. Miao, L. Caron, J. Cedervall, P. Gubbens, P. D. De Réotier, A. Yaouanc, F. Qian, A. Wildes, H. Luetkens, A. Amato *et al.*, Physical Review B **94**, 014426 (2016).
 - [7] N. H. Dung, Z. Q. Ou, L. Caron, L. Zhang, D. T. C. Thanh, G. A. De Wijs, R. A. De Groot, K. J. Buschow, and E. Brück, Advanced Energy Materials **1**, 1215 (2011).
 - [8] J. Lai, B. Huang, X. Miao, N. Van Thang, X. You, M. Maschek, L. van Eijck, D. Zeng, N. van Dijk, and E. Brück, Journal of Alloys and Compounds **803**, 671 (2019).
 - [9] J. Lai, X. You, I. Dugulan, B. Huang, J. Liu, M. Maschek, L. van Eijck, N. van Dijk, and E. Brück, Journal of Alloys and Compounds **821**, 153451 (2020).
 - [10] M. Hudl, L. Häggström, E.-K. Delczeg-Czirjak, V. Höglin, M. Sahlberg, L. Vitos, O. Eriksson, P. Nordblad, and Y. Andersson, Applied Physics Letters **99**, 152502 (2011).
 - [11] V. Höglin, J. Cedervall, M. S. Andersson, T. Sarkar, M. Hudl, P. Nordblad, Y. Andersson, and M. Sahlberg, Rsc Advances **5**, 8278 (2015).
 - [12] C. A. TOPAS, Appl. Crystallogr **51**, 210 (2018).
 - [13] L. Vitos, *Computational quantum mechanics for materials engineers: the EMTO method and applications*, Springer Science & Business Media (2007).
 - [14] J. P. Perdew, K. Burke, and M. Ernzerhof, Physical review letters **77**, 3865 (1996).

- [15] K. A. Gschneidner, V. Pecharsky, and A. Tsokol, Reports on progress in physics **68**, 1479 (2005).
- [16] L. Caron, Z. Ou, T. Nguyen, D. C. Thanh, O. Tegus, and E. Brück, Journal of Magnetism and Magnetic Materials **321**, 3559 (2009).
- [17] S. Ghorai, R. Skini, D. Hedlund, P. Ström, and P. Svedlindh, Scientific Reports **10**, 1 (2020).
- [18] K. Gschneidner Jr and V. K. Pecharsky, Annual Review of Materials Research **30**, 387 (2000).
- [19] B. Shen, J. Sun, F. Hu, H. Zhang, and Z. Cheng, Advanced Materials **21**, 4545 (2009).
- [20] M.-H. Phan and S.-C. Yu, Journal of Magnetism and Magnetic Materials **308**, 325 (2007).
- [21] R. Skini, S. Ghorai, P. Ström, S. Ivanov, D. Primetzhofer, and P. Svedlindh, Journal of Alloys and Compounds **827**, 154292 (2020).
- [22] C.-B. Rong and J. P. Liu, Applied physics letters **90**, 222504 (2007).
- [23] N. Trung, Z. Ou, T. Gortenmulder, O. Tegus, K. Buschow, and E. Brück, Applied Physics Letters **94**, 102513 (2009).
- [24] D. Cam Thanh, E. Brück, N. Trung, J. Klaasse, K. Buschow, Z. Ou, O. Tegus, and L. Caron, Journal of Applied Physics **103**, 07B318 (2008).
- [25] X. Miao, Y. Mitsui, A. I. Dugulan, L. Caron, N. Thang, P. Manuel, K. Koyama, K. Takahashi, N. Van Dijk, and E. Brück, Physical Review B **94**, 094426 (2016).
- [26] M. Boeije, P. Roy, F. Guillou, H. Yibole, X. Miao, L. Caron, D. Banerjee, N. Van Dijk, R. De Groot, and E. Brück, Chemistry of Materials **28**, 4901 (2016).
- [27] X.-F. Miao, S.-Y. Hu, F. Xu, and E. Brück, Rare Metals **37**, 723 (2018).
- [28] N. H. Dung, L. Zhang, Z. Q. Ou, and E. Brück, Scripta Materialia **67**, 975 (2012).
- [29] D. Fruchart, S. Haj-Khlifa, P. de Rango, M. Balli, R. Zach, W. Chajec, P. Fornal, J. Stanek, S. Kaprzyk, and J. Tobola, Crystals **9**, 37 (2019).
- [30] S. Yoon and J. Booth, Physics Letters A **48**, 381 (1974).
- [31] L. Pal, K. Suresh, and A. Nigam, Journal of Applied Physics **113**, 093904 (2013).
- [32] E. K. Delczeg-Czirjak, M. Pereiro, L. Bergqvist, Y. O. Kvashnin, I. Di Marco, G. Li, L. Vitos, and O. Eriksson, Physical Review B **90**, 214436 (2014).
-

Appendix A: Supplementary Information

1. Δc , Δa , and $\Delta(c/a)$ calculation

Fig.6 shows the c lattice parameter values for the dominant ($> 80\%$) Fe_2P phase above and below T_C for the parent compound together with linear fits to describe the temperature dependence. The separation between the fitted lines at T_C , represents the Δc parameter. Similarly, the values of Δa and $\Delta(c/a)$ have been calculated for the three compounds.

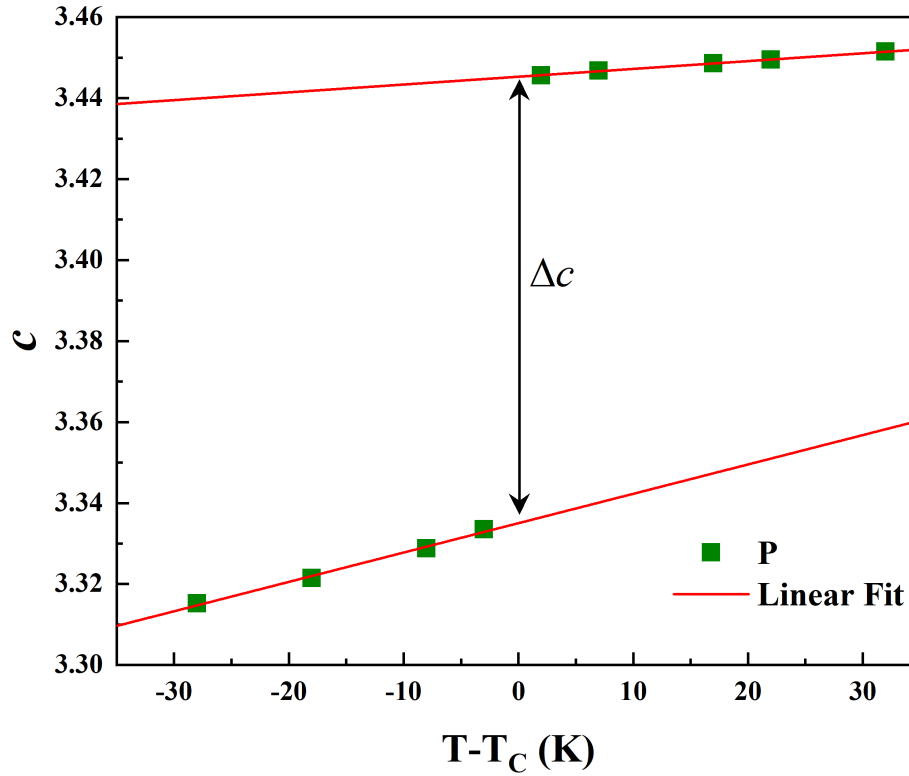


FIG. 6. Temperature dependence of the c lattice parameter for the dominant Fe_2P phase for the parent compound showing how Δc has been defined. Similarly Δc , Δa and $\Delta(c/a)$ have been calculated for all the compounds.

2. Temperature dependent XRPD

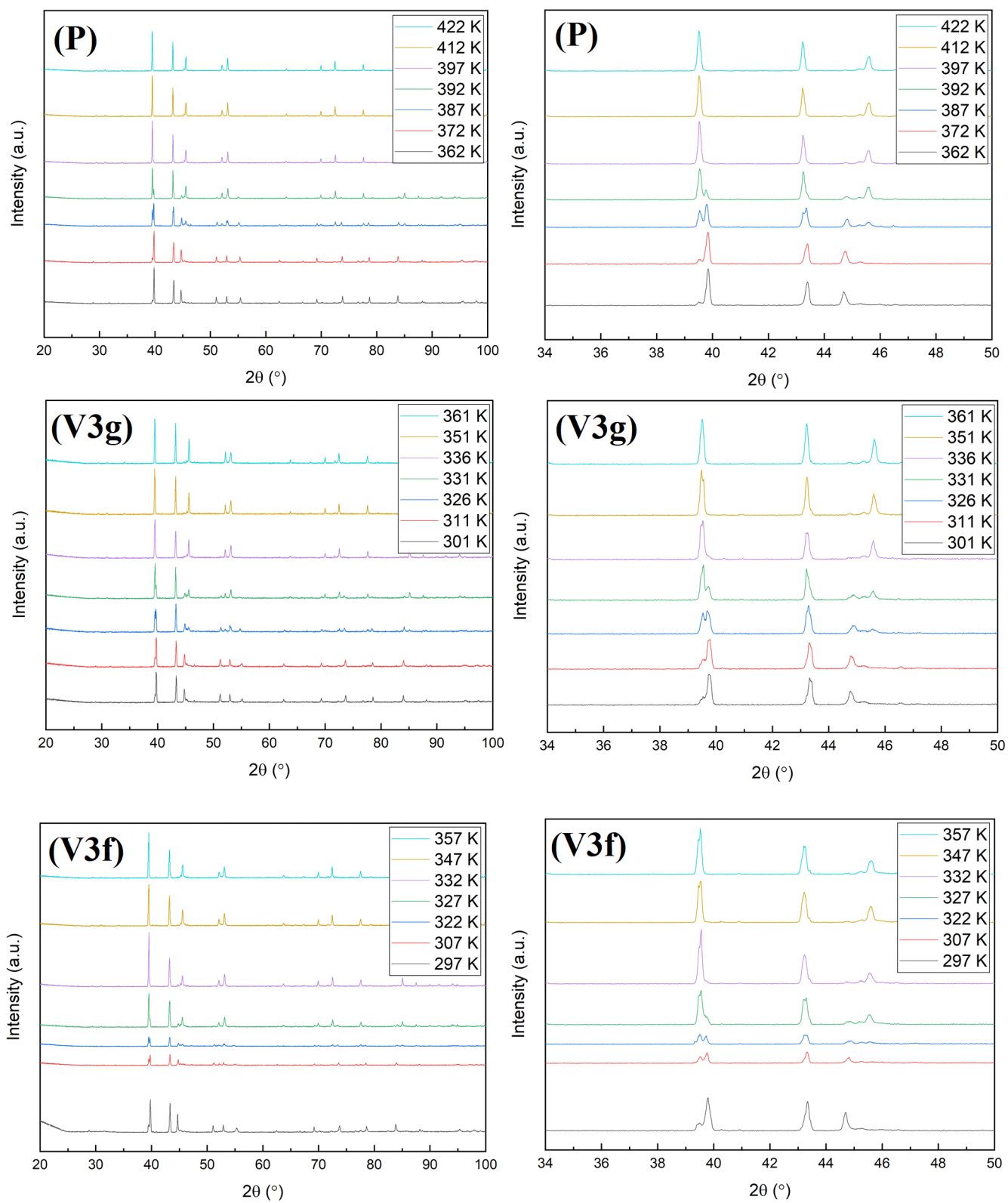


FIG. 7. Temperature dependent XRPD patterns for the three studied compounds.

3. EDX mapping

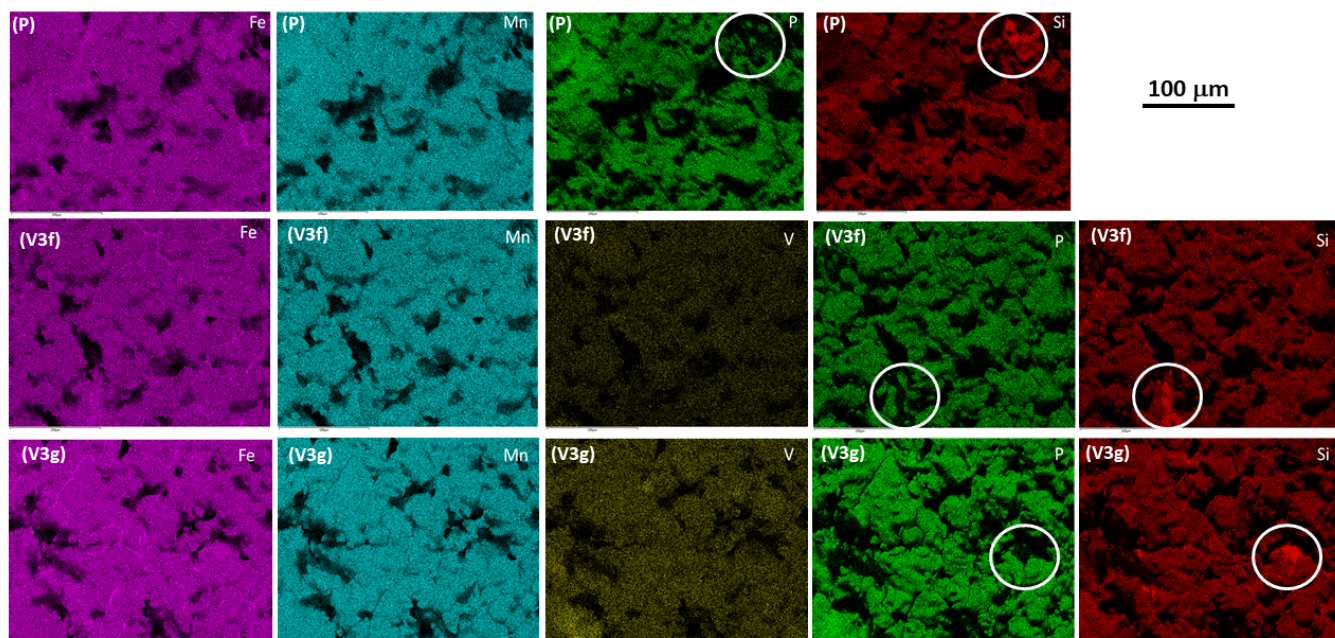


FIG. 8. Elemental mapping of the studied compounds. The circled regions show deficiency of P and excess of Si.